Optical pattern formation in self-focusing and self-defocusing diffractively thick media

G. Labeyrie,[1,*] I. Kresic,[2,3] R. Kaiser,[1] and T. Ackemann[4]
[1]*Université Côte d'Azur, CNRS, Institut de Physique de Nice, 06560 Valbonne, France*
[2]*Institute of Physics, Bijenička Cesta 46, 10000 Zagreb, Croatia*
[3]*Institute for Theoretical Physics, Vienna University of Technology, Vienna 1040, Austria*
[4]*SUPA and Department of Physics, University of Strathclyde, Glasgow G4 0NG, United Kingdom*

(Received 11 February 2025; accepted 21 May 2025; published 4 June 2025)

Cold atomic clouds constitute highly resonant nonlinear optical media, whose refractive index can easily be tuned via the light frequency. When subjected to a retroreflected laser beam and under appropriate conditions, the cloud undergoes spontaneous symmetry breaking, and spatial patterns develop in the transverse cross section of the beam. We investigate the impact of the sign of the light detuning from the atomic resonance on these patterns, thus directly comparing pattern formation for self-focusing and self-defocusing nonlinearities. Our observations emphasize the need for a "diffractively thick" medium description of the light-cloud interaction in which diffraction and nonlinear propagation inside the sample are taken into account.

DOI: 10.1103/PhysRevA.111.063506

I. INTRODUCTION

For a few decades, cold and ultracold atomic ensembles have been extensively used as quantum simulators to investigate solid-state physics. One of the main advantages of these systems is their tunability, implemented through variations of an external parameter. For instance, an externally applied magnetic field can be used to adjust the magnitude and sign of contact interactions between atoms through the use of Feshbach resonances, a technique that has been essential to the investigation of, e.g., the BEC-BCS crossover [1].

Similarly, the optical properties, either linear or nonlinear, of a cold atomic sample can be conveniently tuned by adjusting the laser frequency detuning from an optical line, taking advantage of the sharp resonance. In the present work, we change the sign of the laser detuning to pass from a self-focusing nonlinearity (where the refractive index increases with laser intensity) to a self-defocusing one (where the refractive index decreases with laser intensity). We are then able to investigate the impact of this change on light-induced self-organization due to diffractive coupling [2] without actually modifying the sample. Our observations emphasize the important role played by diffraction and nonlinear refraction inside the cloud in this experiment.

Spontaneous pattern formation in optical systems has been studied for three decades using a variety of platforms such as hot atomic vapors [3–5], liquid crystals [6,7], and photorefractive systems [8,9]. Starting from 2011, cold atomic samples emerged as interesting media in which different kinds of optical nonlinearities can be used for pattern formation [10–12]. In our group, we demonstrated self-organization based on spatial bunching of the cold atoms [11], saturation of the atomic transition [13], and magnetism based on optical pumping [14–16]. These various mechanisms can be selected in the *same* atomic cloud by tuning external parameters, such as the laser intensity and frequency detuning, or an external magnetic field. In the present work, we use magnetic spin-based nonlinearity at zero magnetic field, which leads to the spontaneous appearance of an antiferromagnetic phase with square symmetry [14,15].

The first observations of transverse instability in hot [3] and cold [10] atomic vapors relied on counterpropagating beams interacting with the nonlinear medium. An analysis of this problem is challenging because diffraction and nonlinearity act simultaneously. Semianalytical results were obtained for the length scales and the threshold of the instability under simplified conditions [3,8,17], but to our knowledge only one numerical simulation was ever performed due to the high demand for computational resources [18]. The system suggested in [2] is conceptually much simpler. The pump beam passes through a nonlinear medium that is sufficiently thin for diffraction not to be significant. Then diffraction takes places in vacuum (without nonlinearity) between the medium and a retroreflecting feedback mirror (for details see Sec. II). Due to this separation between nonlinearity and diffraction, this system is easily tractable analytically and numerically, e.g., [2,12,19,20]. It is now natural to ask what happens when this separability breaks down, i.e., when the feedback-mirror distance is reduced such that diffraction within the medium become non-negligible. This problem arises already in the context of linear optics because it is related to the transition between Raman-Nath diffraction from "thin" gratings and Bragg diffraction from "thick" gratings (e.g., [21]) and in atom optics in the transition between Kapitza-Dirac and Bragg diffraction (e.g., [22]). Hence, it also has relevance to understanding the different regimes of superradiance in nonlinear atom optics [23,24]. There is also a temporal analog for the single-mirror-feedback system based on nonlinear fiber optics and dispersion replacing diffraction, and "diffraction" within the nonlinear medium can be important [25]. In a more general setting the interaction of Talbot-like self-imaging phenomena

*Contact author: guillaume.labeyrie@univ-cotedazur.fr

 ©2025 American Physical Society

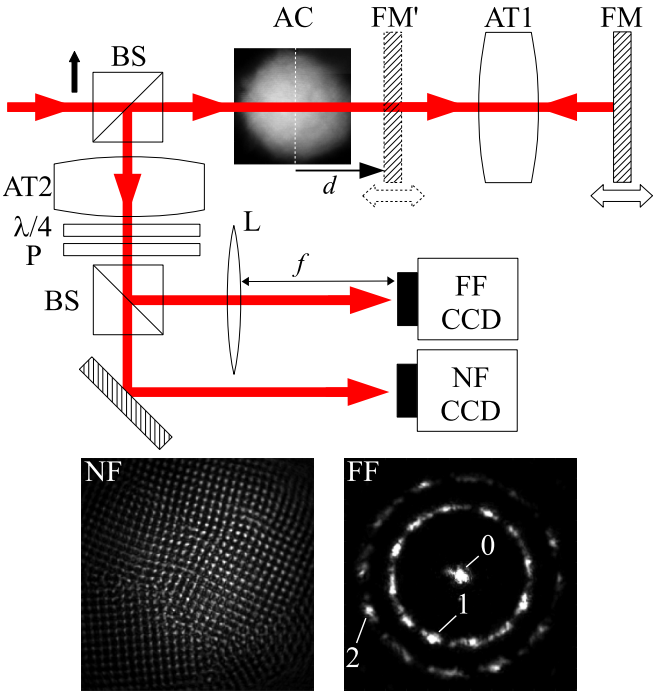


FIG. 1. Experimental setup. A laser beam is sent through a laser-cooled atomic cloud (AC) and retroreflected by a feedback mirror (FM) on a translation stage. An afocal telescope (AT1) is used to image a "virtual feedback mirror" (FM′) at a distance d from the cloud. The reflected light is collected by a beam splitter (BS), passed through a circular polarization analyzer (quarter-wave plate $\lambda/4$ + polarizer P), divided into two parts by a BS and directed on two CCDs used to record the transverse intensity distributions of the light in both the near field (NF) and far field (FF; 0: on-axis pump, 1: first off-axis wave number, 2: second off-axis wave number).

and nonlinearity has been discussed in relation to harmonic generation [26] and nonlinear fiber optics [27,28] and is often referred to as the nonlinear Talbot effect.

We first describe our experiment and the principles behind self-organization due to diffractive coupling. We then present the results of an experiment in which the feedback distance is varied across positive and negative values for two values of laser detuning with opposite signs. We then discuss these results based on both a thin-medium model [2] and a more involved thick-medium one [29].

II. EXPERIMENT

We use a modified version of our previous setup [11,13,14] sketched in Fig. 1 based on the single-feedback-mirror scheme introduced by Firth in 1990 [2]. A large cloud of cold ^{87}Rb (FWHM $L = 12$ mm, optical density at resonance $= 130$, temperature $= 200$ μK) is produced in a vapor-loaded magneto-optical trap (MOT). We then shut down the MOT and send a "pump" laser beam with a waist of 2.2 mm through the cloud. This beam is linearly polarized, with a detuning (either positive or negative) $|\delta| = 10.4\,\Gamma$ from the $F = 2 \to F' = 3$ transition, where Γ is the natural width. The peak intensity is $I_0 = 13$ mW/cm^2, which corresponds to a saturation parameter $s = \frac{I/I_{\rm sat}}{1+4(\delta/\Gamma)^2} = 0.008$ (assuming a saturation intensity $I_{\rm sat} = 3.58\,$mW/cm^2 for unpolarized atoms). The beam is applied for a duration of 1 ms, with the detection (image acquisition) taking place in the last 100 μs of this pulse. The beam transmitted by the cloud (corresponding to 75% of the incident) is retroreflected by a "feedback mirror" set on a translation stage, located outside the vacuum chamber. An afocal telescope (AT1) is used to create a "virtual" mirror near the cloud (i.e., inside the vacuum chamber) by imaging the real one. This arrangement allows us to have access to a small, effective cloud-mirror distance d, as well as negative values [7] (see Fig. 4 below). As will be seen, the sign of d plays an important role in the observations. After passing again through the cloud, part of the retroreflected beam is collected by a nonpolarizing beam splitter for pattern detection. We select circularly polarized light with the help of a quarter-wave plate and a polarizer. We then split this light into two parts that are directed to two CCD cameras to detect both the near-field (NF) and far-field (FF) intensity distributions simultaneously. The NF imaging is achieved through another afocal telescope (AT2), with the FF imaging requiring an additional lens (L). During the interaction of the laser beam with the atoms, the magnetic field is set to $B = 0$.

Most measured quantities presented in this paper are extracted from far-field images (i.e., optical Fourier spectra), as shown in Fig. 1. The central spot corresponds to the pump beam. Above the instability threshold, it is surrounded by bright dots distributed on several circles corresponding to different spontaneously generated transverse modes. In the following we will refer to the collection of spots on a given circle as a "mode," as we are interested only in the transverse wave number. Two such modes are visible in the FF image in Fig. 1, labeled 1 and 2. The radius of each circle corresponds to a diffracted angle $\theta_d = q/k = \lambda/\Lambda$, where $q = 2\pi/\Lambda$ is the transverse wave number and Λ is the modulation wavelength in the transverse plane (determining the size of the pattern's unit cell in the NF). We see in the NF image in Fig. 1 that the patterns have a clear square symmetry but that the beam's cross section is divided into several domains with different pattern orientations ("polycrystalline pattern"). Hence, the corresponding FF image exhibits here 12 spots (three sets of four spots). To perform the FF analysis, we first average 10 single-shot FF images. Each shot corresponds to a new MOT. Since both translational and rotational degrees of freedom are almost unconstrained in the patterns (the Gaussian shape of the input laser beam provides only a weak pinning of the position), the position and orientation of the patterns vary from shot to shot. As a result, the averaged FF image shows an intensity distributed more or less uniformly along a circle of radius θ_d. By measuring θ_d we obtain q and thus Λ. We also extract the diffracted power P_d, obtained by integrating the FF image around the circle. This quantity provides an indication of the distance to the instability threshold (the larger P_d is, the larger the distance to the threshold is), although it is not as direct as measuring the threshold intensity, which is more time-consuming.

As mentioned earlier, the present work is based on the magnetic optical pumping nonlinearity [14–16], in which the patterns are due to a spatial modulation of the Zeeman populations in the ground state (orientation). These patterns

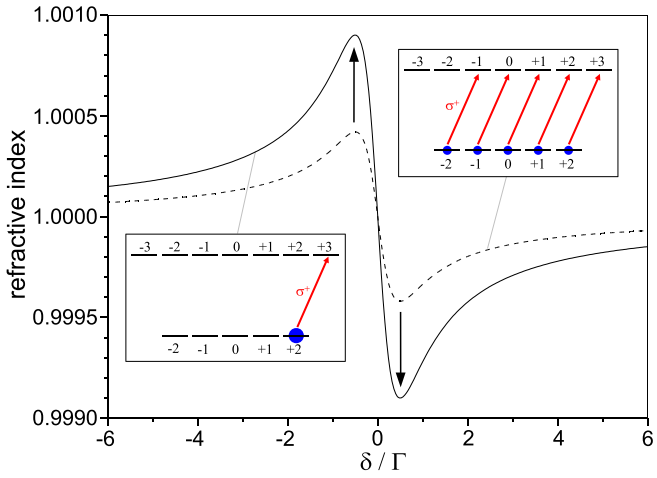


FIG. 2. Nature of the optical pumping nonlinearity. We plot the refractive index of the cold cloud versus light detuning for an atomic density $\rho = 10^{11}$ cm^{-3} and circular polarization of the light. The dashed line corresponds to atoms evenly distributed among Zeeman sublevels, corresponding to a degeneracy factor $g = 7/15$. The solid line corresponds to atoms fully pumped in the stretched state. This can be obtained by slightly increasing the light intensity I to overcome, e.g., the redistribution effect of stray magnetic fields. Thus, the refractive index increases with I for $\delta < 0$ (self-focusing nonlinearity) and decreases when I increases for $\delta > 0$ (self-defocusing nonlinearity), as shown by the arrows.

are very sensitive to the magnetic field, which needs to be controlled within the 10 mG range. When the magnetic field is set to zero, the system self-organizes into an antiferromagnetic phase in which atoms are optically pumped in the stretched states. Because the Clebsch-Gordan coefficients are maximal in these stretched states, this optical pumping nonlinearity is self-focusing (i.e., the refractive index increases with light intensity) for red detunings ($\delta < 0$) and self-defocusing for blue ones ($\delta > 0$). This is illustrated in Fig. 2, where we plot the (linear) refractive index for a cold cloud with an even population distribution in the Zeeman substates of the ground state (dashed line) and the same for a cloud optically pumped in the stretched state $m_F = +2$ (solid line). The optical pumping results in an increase of the refractive index for $\delta < 0$ and a decrease for $\delta > 0$. Note that this is opposite to the case of the standard two-level nonlinearity [13]. Since the nonlinearity used in this work is based on the very efficient process of optical pumping, the associated intensity instability threshold is very low compared to that of instabilities based on other nonlinear mechanisms such as saturation [13] and optomechanics [11]. Thus, the width of the dispersion curve for the cloud's refractive index is close to the natural width ($\Gamma/2\pi \approx 6$ MHz), and one can conveniently pass from a self-focusing nonlinearity to a self-defocusing one by tuning the frequency of the light by a few tens of megahertz without modifying the size or geometry of the cloud.

The expected impact of the sign of the detuning on self-organization is twofold. First, it affects the spatial period of the patterns. Indeed, in the thin-medium model of diffractive coupling providing the optical feedback [2], diffraction within the medium is neglected, and only the propagation of light in free space between the sample and mirror and back with a length $2d$ converts a pure phase modulation into a pure amplitude modulation. A positive feedback is obtained after round-trip propagation of $Z_T/4$ in the self-focusing case and $3Z_T/4$ in the self-defocusing case [12], where $Z_T = 2\Lambda^2/\lambda$ is the so-called Talbot length. These conditions for positive feedback, necessary for the establishment of the so-called Talbot modes, can be summarized as follows. For a self-focusing nonlinearity (here for $\delta < 0$),

$$d = (1/4 + n)\frac{\Lambda^2}{\lambda}, \tag{1}$$

with n being an integer (positive or negative depending on the sign of d). For a self-defocusing nonlinearity ($\delta > 0$),

$$d = (3/4 + n)\frac{\Lambda^2}{\lambda}. \tag{2}$$

The value of the integer n determines which mode is considered. For instance, for the self-focusing case [Eq. (1)] and $d > 0$, n can take any positive value. The lowest-q (largest-Λ) mode corresponds to $n = 0$. For $d < 0$, n is negative, and the lowest-q mode corresponds to $n = -1$. For these two cases, the corresponding diffraction angles thus are

$$\theta_d = \sqrt{\frac{\lambda}{4d}}, \quad d > 0, \tag{3}$$

and

$$\theta_d = \sqrt{-\frac{3\lambda}{4d}}, \quad d < 0. \tag{4}$$

The reverse applies for a self-defocusing nonlinearity:

$$\theta_d = \sqrt{\frac{3\lambda}{4d}}, \quad d > 0, \tag{5}$$

and

$$\theta_d = \sqrt{-\frac{\lambda}{4d}}, \quad d < 0. \tag{6}$$

Second, the sign of the detuning may affect the stability of the patterns due to nonlinear propagation effects taking place inside the cold-atom cloud. Indeed, our system cannot be expected to behave according to the thin-medium regime when d is of the order of the thickness L of the cloud. On the contrary, in this thick-medium regime effects such as diffraction and nonlinear refraction take place within the cloud. Indeed, the bright spots seen in Fig. 3 can be individually seen as Gaussian beams with a waist of the order of a few tens of microns. Self-focusing or defocusing can then occur within the thickness of the cloud. Self-focusing is expected to balance diffraction and help stabilize the transverse size of the individual spots, while the opposite should occur for the self-defocusing situation [30]. We thus expect instability threshold intensities for $\delta > 0$ to be substantially higher than for $\delta < 0$.

III. RESULTS

Figure 3 shows examples of NF images of patterns obtained for opposite values of the detuning ($|\delta| = 10.4\,\Gamma$) and a negative feedback distance, $d = -24.2$ mm. Since the optical thickness of the cloud is symmetrical with respect to the sign

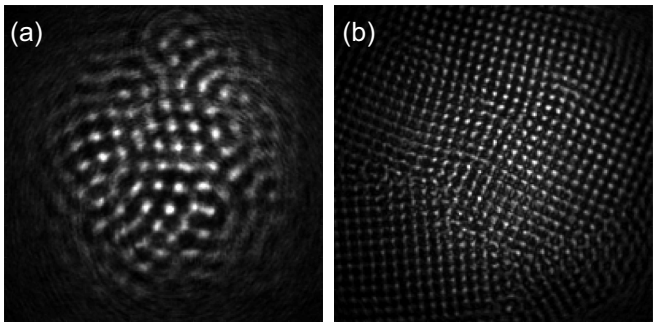


FIG. 3. Comparison of red and blue patterns (near field). (a) NF image for $\delta = +10.4\,\Gamma$. (b) NF image for $\delta = -10.4\,\Gamma$. The field of view is 3.6 mm. The parameters are $d = -24.2$ mm, $I_0 = 13$ mW/cm^2, and $B = 0$.

of δ, the only change between the two situations is due to the refractive index, which is dispersive (see Fig. 2). As can be seen, the spatial scale Λ of the patterns is larger for $\delta > 0$ than for $\delta < 0$. According to the discussion above, this observation confirms that the nonlinearity is self-focusing for $\delta < 0$ and self-defocusing for $\delta > 0$.

A more quantitative comparison is provided in Fig. 4, where we report the measured diffraction angle θ_d versus feedback distance d for both $\delta < 0$ (red circles, dots, and stars) and $\delta > 0$ (blue squares). For comparison, we also plot the thin-medium predictions for a self-focusing nonlinearity (red solid lines) and a self-defocusing nonlinearity (blue dashed lines), as obtained from Eqs. (3)– (6). The bold vertical lines delimit the FWHM extent of the cloud, but it should be stressed that the spatial density profile is not uniform but close to Gaussian. For clarity, we restrict the data presented in Fig. 4

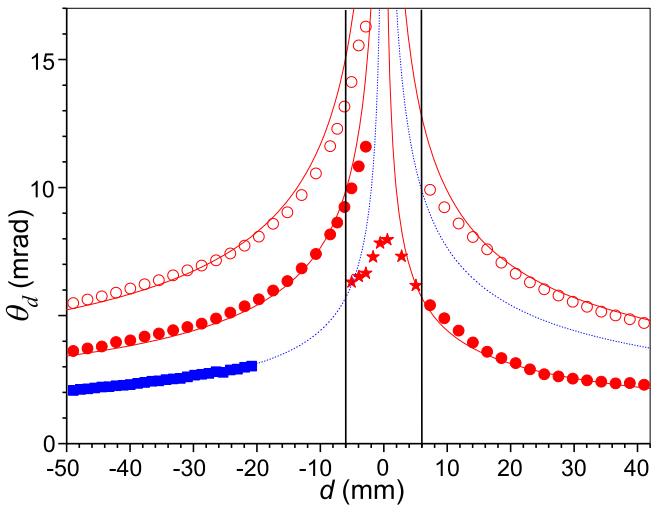


FIG. 4. Diffraction angle θ_d versus feedback-mirror distance d. We report experimental measurements for the lowest-q modes for $\delta < 0$ (circles) and $\delta > 0$ (squares). The solid red and dashed blue lines correspond to the thin-medium model predictions for self-focusing and self-defocusing nonlinearities, respectively. When the effective mirror is inside the cloud (delimited by the bold vertical lines), we observe strong deviations from the thin-medium model ($\delta < 0$, stars).

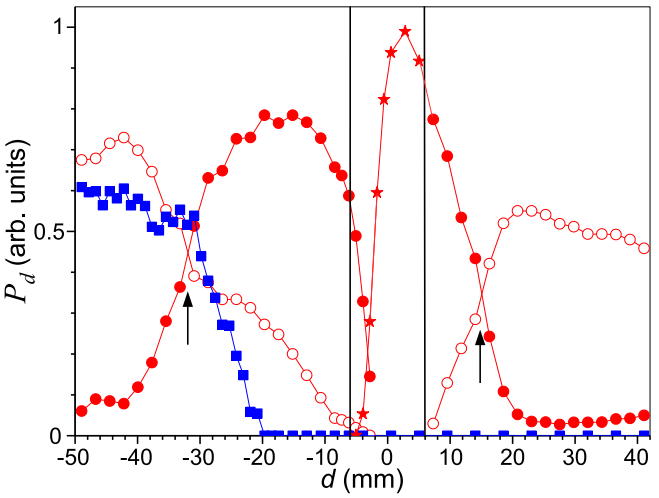


FIG. 5. Measured diffracted power P_d versus feedback-mirror distance for the data in Fig. 4. The choice of symbols is the same as in Fig. 4. The bold vertical lines delimitate the FWHM extent of the cloud. The arrows mark the positions of crossover between the two modes for $\delta < 0$.

to the two lowest-q modes for $\delta < 0$ (except in the narrow range $-6 < d < -4$ mm, where three modes are shown) and to the lowest-q mode for $\delta > 0$. Note, however, that we can observe up to eight modes for $\delta < 0$ and large values of $|d|$ but only two modes for $\delta > 0$ (the second one is much weaker).

Looking first at the $\delta < 0$ case, we see that when $|d|$ is large enough, the measured θ_d closely matches the thin-medium prediction. Note that the only adjustable parameter for this experiment-model comparison is the position $d = 0$, which is difficult to measure accurately in the experiment because of the large size of the cloud. A small global horizontal translation of the experimental curves is thus allowed to optimize the match.

When $|d|$ decreases below a certain value (which increases with the order of the considered mode), the measured θ_d starts to deviate from thin-medium theory. When the effective feedback mirror is inside the cloud, this deviation becomes very important (see the stars in Fig. 4), and θ_d tends to saturate to a finite value for $d \approx 0$. This behavior was discussed in Ref. [20]: When $|d| \gg L$, the pattern's period Λ is determined by feedback from the mirror and thus varies with d, while for $|d| < L$ it is the thickness of the sample that is the relevant length scale like in the situation with independent counter-propagating beams [3,17] and $\Lambda = \sqrt{2L\lambda}$. Using the cloud's FWHM size $L = 12$ mm, we get $\theta_d = 5.7$ mrad, which is not too far from the saturation value observed in Fig. 4. Of course, a quantitative difference is expected between the homogeneous slab geometry and that of a Gaussian density profile. Looking in detail at Fig. 4 around $d = 0$, we observe a rather complex behavior with a smooth transition from thin-medium behavior to progressive saturation on the $d > 0$ side and an abrupt mode jump occurring around $d = -6$ mm. We will discuss these observations later (see Fig. 6 below).

For $\delta > 0$ the situation is markedly different. The lowest-q mode is observed only for large, negative feedback distances $d < -20$ mm. No patterns are observed for $d > 0$ (see below

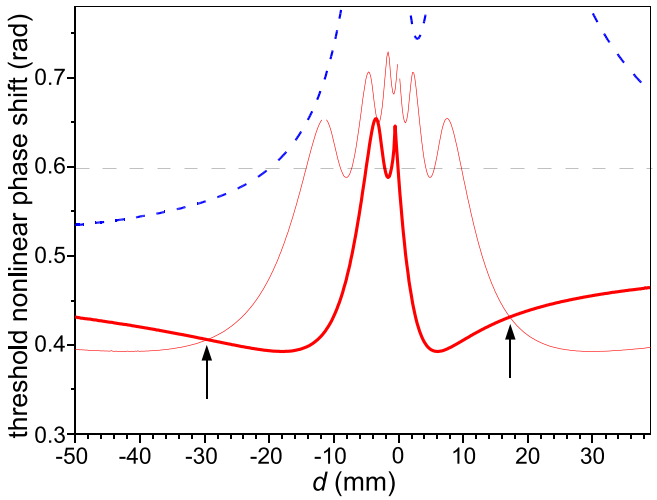


FIG. 6. Threshold nonlinear phase shift versus feedback-mirror distance as predicted by the thick-medium model. The thick and thin red curves correspond to the first and second lowest-q modes for $\delta < 0$, respectively. The arrows mark the positions of crossover between these two modes. The dashed blue curve corresponds to the lowest-q mode for $\delta > 0$. The horizontal dashed line marks the approximate value of the nonlinear phase shift in the experiment (see text).

for a discussion of this striking asymmetry). For $d < -20$ mm, the agreement with the thin-medium theory is excellent, confirming the self-defocusing nature of the nonlinearity for $\delta > 0$.

To complement the data in Fig. 4, we plot in Fig. 5 the diffracted power P_d versus d using the same choice of symbols. For $\delta < 0$, we observe the following general behavior for the Talbot modes (red dots and circles), including the higher-q modes not shown here: The curves $P_d(|d|)$ are bell shaped and reach their maxima for values of $|d|$ that increase with the order of the Talbot modes. As a consequence, when increasing $|d|$ from zero, we observe that the order of the dominant mode (i.e., that with the largest P_d) increases. The transition between the first and second Talbot modes occurs in Fig. 5 for $d = -32$ mm and $d = +15$ mm (arrows), so there is an asymmetry between $d > 0$ and $d < 0$. This behavior of the transition between successive dominant modes as $|d|$ is increased was already observed in another experiment using the same optical pumping nonlinearity but different parameters (see Fig. 15(b) in [29]).

IV. DISCUSSION

The behaviors observed in Fig. 5 (and in Fig. 4 for small enough values of $|d|$) cannot be understood using the thin-medium theory. In Ref. [29], we described a thick-medium model based on a two-level description of the atom-light interaction (the saturable Kerr model). This model, in its most complete form, includes nonlinear absorption and propagation effects as well as diffraction inside the sample and the presence of transverse and longitudinal gratings due to the interference between all light beams. In the simplified version used in this paper, we implemented the "quasi-Kerr approximation" obtained by neglecting absorption, as described in Sec. VII of Ref. [29]. In this regime, it is possible to derive an expression for the instability intensity threshold. The details of this derivation are given in the Appendix. We stress that since the nonlinearity at work in this paper is based on Zeeman optical pumping instead of the saturation of a two-level atomic transition, we do not expect quantitative agreement between theory and experiment, for instance, for the threshold intensities.

In the framework of this model, complex oscillatory behavior of the instability threshold with both the pattern's transverse wave vector q and the feedback distance d is predicted, causing the observed alternation of dominant Talbot modes as d is scanned. In contrast, in the case of self-defocusing, the thick-medium model predicts a continuous decrease of the Talbot mode thresholds as $|d|$ increases, which is consistent with the observations reported in Fig. 5 for $\delta > 0$.

As already stressed above, a striking result of our experiment is the absence of patterns for $\delta > 0$ and $d > 0$. To try to understand this observation, we compare in Fig. 6 the intensity threshold curves versus d, derived from our thick-medium model (see the Appendix for details) for both $\delta < 0$ and $\delta > 0$. We plot in Fig. 6 the nonlinear phase shift at the instability threshold, which is proportional to the threshold intensity. The thick and thin red curves correspond to the first and second lowest-q modes for $\delta < 0$, respectively. The dashed blue curve corresponds to the lowest-q mode for $\delta > 0$.

It is important to realize that the thin-medium theory for a local Kerr medium as considered here predicts a threshold nonlinear phase shift of 0.5, independent of the wave number and hence of d. Looking at Fig. 6, we see that the thick-medium threshold for the lowest-q mode is considerably lower than 0.5 for the focusing medium (except for small $|d|$) and larger for the defocusing medium. This makes sense because self-focusing will stabilize spots into tubes along the whole longitudinal extent of the medium, whereas self-defocusing will destabilize these tubes.

For $\delta < 0$, we observe a crossover between the two lowest-q modes for $d \approx -30$ mm and $d \approx +17$ mm (arrows in Fig. 6), with the lowest-q mode being dominant for $-30 < d < 17$ mm (the lowest intensity threshold). This is in excellent agreement with the experimental observation in Fig. 5. We note that the asymmetry between $d < 0$ and $d > 0$ is well reproduced by the model.

We now turn to the even stronger asymmetry observed for $\delta > 0$. The fixed intensity I_0 used in the experiment corresponds to the horizontal line in Fig. 6. Whenever the threshold intensity for a given mode is below I_0, this mode is observed. As stressed before, we do not have a quantitative model to link the nonlinear phase shift to the laser intensity in the case of the magnetic optical pumping nonlinearity. We thus position the horizontal dashed line in Fig. 6 to match the region where patterns are observed for $\delta > 0$ ($d < -20$ mm). Once this is set, we see that patterns for $\delta > 0$ cannot be observed in the rest of the explored d range, while for $\delta < 0$ patterns are observed throughout most of the d range (with some oscillations around $d = 0$). The thick-medium model thus provides an accurate description of our experimental observations. Extrapolating on the dashed blue curve in Fig. 6, one would expect to be able to observe patterns for $\delta > 0$ at the same laser

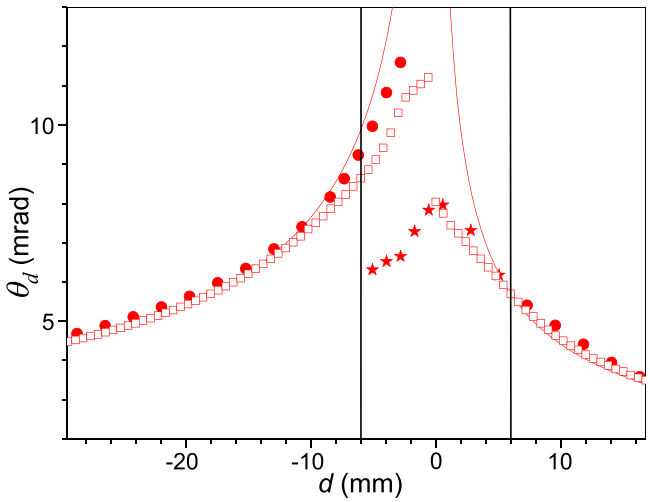


FIG. 7. Comparison between experiment and the thick-medium model. We show the data in Fig. 4 for $\delta < 0$ (lowest-q mode, solid dots and stars) and a restricted range around $d = 0$. The red solid lines correspond to the thin-medium model. The squares are obtained from the thick-medium model.

intensity but for a larger positive d (not feasible with the actual setup) or by setting, e.g., $d = +40$ mm and increasing I_0. We tried the latter without success. We thus conclude that some additional effect not included in our thick-medium model further prevents pattern formation for $\delta > 0$ and $d > 0$. We also measured the threshold intensities for $\delta > 0$ and $\delta < 0$ for $d = -50$ mm and found that the threshold intensity for $\delta > 0$ is 2 times larger than for $\delta < 0$. This ratio is quite a bit larger than what is reported in Fig. 6. The likely effect missing in the current description is the residual motion of the atoms, leading to an increase in the threshold with increasing q. The interplay of this effect with the self-defocusing in the medium is likely to suppress the instability. However, its modeling would be quite involved and is outside the scope of this paper.

Finally, in Fig. 7 we compare the experimentally measured θ_d to the thick-medium prediction. The dots and stars correspond to the experimental data for the lowest-q mode as in Fig. 4; the red curves show the thin-medium theory. The open squares are obtained with the thick-medium model. While the agreement is not perfect, the main features (saturation and mode jump) are well reproduced.

V. CONCLUSION

In this work, we used the resonant character of the nonlinear refractive index of a cold atomic cloud to directly compare optical pattern formation for self-focusing and self-defocusing nonlinearities in the single-feedback-mirror configuration. We found that the pattern's respective sizes in the two situations are in quantitative agreement with predictions of the thin-medium model when the feedback distance d is large compared to the cloud's size L. However, even in this range of feedback distances, thick-medium effects manifest through the d dependence of threshold intensities for the different Talbot modes. The strong red-blue asymmetry observed in this work, with a much reduced range of pattern formation on the self-defocusing side ($\delta > 0$), highlights the importance of self-focusing inside the cloud to promote pattern formation. This is further confirmed by observations reported in [13] for the two-level nonlinearity, where a similar asymmetry was observed but with the opposite sign.

We also reported a detailed experimental observation of the behavior of the pattern size around $d = 0$ in a diffractively thick medium. When the effective feedback mirror was inside the cloud, we observed strong deviations from the thin-medium model even for the period of the patterns, which does not decrease to zero but saturates at a finite minimum value. This behavior can be expected because the medium thickness becomes the relevant diffractive length scale once the mirror distance is small. A complex asymmetric behavior including mode jumps, which is qualitatively reproduced by the local thick-medium model but whose quantitative understanding requires further investigation, was observed. In particular, the inclusion of wave-number-dependent losses due to the residual atomic motion is expected to improve the theoretical description.

These investigations provide insight into the transition out of the Raman-Nath regime for nonlinear grating. They might also be important for understanding the limits of storing images and structured quantum information in atomic samples.

ACKNOWLEDGMENTS

The Nice group acknowledges support from CNRS, UNS, and Région PACA. I.K. acknowledges support from the project KODYN financed by the European Union through the National Recovery and Resilience Plan 2021–2026 and the project Centre for Advanced Laser Techniques (CALT), cofunded by the European Union through the European Regional Development Fund under the Competitiveness and Cohesion Operational Programme (Grant No. KK.01.1.1.05.0001).

DATA AVAILABILITY

The data that support the findings of this article are not publicly available. The data are available from the authors upon reasonable request.

APPENDIX: DERIVATION OF THE THICK-MEDIUM THRESHOLD EQUATION

Here we recount the derivation of the threshold curve for the quasi-Kerr case of the thick-medium model, given in [29], following the framework of linear-stability analysis described in [17]. We start with the paraxial wave equations for the forward field F and backward field B inside the quasi-Kerr nonlinear medium:

$$\frac{\partial F}{\partial z} - \frac{iL}{2k}\nabla_\perp F = -\frac{i\Delta\alpha_l L}{2}(1 + |F|^2 + |B|^2)F,$$
$$\frac{\partial B}{\partial z} + \frac{iL}{2k}\nabla_\perp B = \frac{i\Delta\alpha_l L}{2}(1 + |F|^2 + |B|^2)B, \qquad \text{(A1)}$$

where $\Delta = 2\delta/\Gamma$, the electric field intensity is normalized to the detuned saturation intensity of the transition $I_{s,\Delta} = I_s/(1 + \Delta^2)$, z is in units of the medium length L, and

$\alpha_l = \alpha_0/(1+\Delta^2)$, with $\alpha_0 L$ being the medium's optical density. Here, we have neglected the medium's absorption (quasi-Kerr limit) along with the reflection grating (i.e., $G = 1 + h = 1$ in [29]). The latter can be neglected because the nonlinearity is sufficiently slow that this small-period longitudinal grating is washed out by atomic motion during the pattern-formation dynamics.

For the homogeneous case the solutions are

$$F_0(z) = F_0 \exp\left[-\frac{i\Delta\alpha_l L}{2}(1+|F_0|^2+|B_0|^2)z\right],$$
$$B_0(z) = B_0 \exp\left[\frac{i\Delta\alpha_l L}{2}(1+|F_0|^2+|B_0|^2)z\right]. \tag{A2}$$

Writing $F(x,z) = F_0[1 + f\cos(qx)]$ and $B(x,z) = B_0[1 + b\cos(qx)]$ leads to equations for the transverse perturbation functions f and b:

$$\frac{\partial f}{\partial z} = -i\theta f + i\Delta\alpha_l L(|F_0|^2 f' + |B_0|^2 b'),$$
$$\frac{\partial b}{\partial z} = i\theta f - i\Delta\alpha_l L(|F_0|^2 f' + |B_0|^2 b'), \tag{A3}$$

where $f = f' + if''$, $b = b' + ib''$, and $\theta = q^2 L/2k$ is the diffractive phase shift between f and F_0 after traversing the length of the optical medium. The full system of equations can be written in matrix form for vector $\mathbf{r} = (f', b', f'', -b'')$:

$$\frac{\partial \mathbf{r}}{\partial z} = \theta \hat{M}\mathbf{r}, \tag{A4}$$

where the matrix $\hat{M}$ has the form

$$\hat{M} = \begin{pmatrix} 0 & \mathbf{I}_2 \\ -\hat{C} & 0 \end{pmatrix}, \quad \hat{C} = \begin{pmatrix} 1-\varphi & -\beta \\ -\varphi & 1-\beta \end{pmatrix}, \tag{A5}$$

with $\beta = \Delta\alpha_l L|B_0|^2/\theta$ and $\varphi = \Delta\alpha_l L|F_0|^2/\theta$. In the following we set $|F_0|^2 = |B_0|^2 = I_0/I_{s,\Delta}$, leading to $\varphi = \beta = \Delta\alpha_l L|F_0|^2/\theta$. Equation (A4) can be integrated to give $\mathbf{r}(z) = \exp(\theta\hat{M}z)\mathbf{r}(0)$, where the exponential function of $\hat{M}$ at $z = 1$ (the end of the optical medium) can be readily calculated to give

$$\exp(\theta\hat{M}) = \begin{pmatrix} \cos\theta\hat{c} & \hat{c}^{-1}\sin\theta\hat{c} \\ -\hat{c}\sin\theta\hat{c} & \cos\theta\hat{c} \end{pmatrix}, \tag{A6}$$

where $\hat{c}^2 = \hat{C}$. Note that even though $\hat{c}$ is not a uniquely defined matrix, the elements of $\exp[\theta\hat{M}]$ are even functions of $\hat{c}$; i.e., they are uniquely defined matrices. Any analytical function $g(\hat{C})$ of $\hat{C}$ can be written using Sylvester's formula for 2×2 matrices, leading to

$$g(\hat{C}) = \begin{pmatrix} 0 & -\varphi \\ -\varphi & 0 \end{pmatrix}\frac{[g(\alpha_1) - g(\alpha_2)]}{\alpha_1 - \alpha_2} + \frac{\mathbf{I}_2}{2}[g(\alpha_1) + g(\alpha_2)], \tag{A7}$$

where α_j are eigenvalues of $\hat{C}$, given by $\alpha_{1,2} = (1, 1-2\varphi)$. This expression can be used to evaluate $\exp(\theta\hat{M})$. Boundary conditions for the single-mirror-feedback system are $f(0) = 0$ and $b(1) = e^{-2i\psi_D} f(1)$, where $\psi_D = D\theta$ and $D = d/L - 1/2$ is the normalized mirror distance from the end of the optical medium. Implementing the boundary conditions via $\mathbf{r}(1) = \exp(\theta\hat{M})\mathbf{r}(0)$ leads to a system of equations:

$$\begin{aligned} f'(1) &= (\cos\theta\hat{c})_{12} b'(0) - (\hat{c}^{-1}\sin\theta\hat{c})_{12} b''(0), \\ f'(1)\cos 2\psi_D + f''(1)\sin 2\psi_D &= (\cos\theta\hat{c})_{22} b'(0) - (\hat{c}^{-1}\sin\theta\hat{c})_{22} b''(0), \\ f''(1) &= -(\hat{c}\sin\theta\hat{c})_{12} b'(0) - (\cos\theta\hat{c})_{12} b''(0), \\ f'(1)\sin 2\psi_D - f''(1)\cos 2\psi_D &= -(\hat{c}\sin\theta\hat{c})_{22} b'(0) - (\cos\theta\hat{c})_{22} b''(0). \end{aligned} \tag{A8}$$

After some algebra, these equations lead to the single-mirror-feedback thick-medium threshold condition [29]:

$$c_1 c_2 + \left(\frac{\psi_2}{\psi_1}c_D^2 + \frac{\psi_1}{\psi_2}s_D^2\right)s_1 s_2 = c_D s_D(\beta_1 s_1 c_2 - \beta_2 s_2 c_1), \tag{A9}$$

where $\psi_1 = \theta$, $\psi_2 = \sqrt{\theta(\theta + 2\Delta\alpha_l L I_0/I_{s,\Delta})}$ [from $\alpha_i = (\psi_i/\theta)^2$], $s_i = \sin\psi_i$, $c_i = \cos\psi_i$, $s_D = \sin\psi_D$, $c_D = \cos\psi_D$, and $\beta_i = (\frac{\psi_i}{\theta} - \frac{\theta}{\psi_i})$. Solving Eq. (A9) leads to the threshold values of the diffractive phase shift θ and nonlinear phase shift $\Delta\alpha_l L I_0/I_{s,\Delta}$. To make a comparison with the experimental results, the diffractive phase shift is converted to the diffracted angle θ_d using $\theta_d = \sqrt{2\theta/kL}$.

[1] T. Bourdel, L. Khaykovich, J. Cubizolles, J. Zhang, F. Chevy, M. Teichmann, L. Tarruell, S. J. J. M. F. Kokkelmans, and C. Salomon, Experimental study of the BEC-BCS crossover region in lithium 6, Phys. Rev. Lett. **93**, 050401 (2004).

[2] W. J. Firth, Spatial instabilities in a Kerr medium with single feedback mirror, J. Mod. Opt. **37**, 151 (1990).

[3] G. Grynberg, E. Le Bihan, P. Verkerk, P. Simoneau, J.R.R. Leite, D. Bloch, S. Le Boiteux, and M. Ducloy, Observation of instabilities due to mirrorless four-wave mixing oscillation in sodium, Opt. Commun. **67**, 363 (1988).

[4] G. Grynberg, A. Maître, and A. Petrossian, Flowerlike patterns generated by a laser beam transmitted through a rubidium cell with single feedback mirror, Phys. Rev. Lett. **72**, 2379 (1994).

[5] T. Ackemann and W. Lange, Non- and nearly hexagonal patterns in sodium vapor generated by single-mirror feedback, Phys. Rev. A **50**, R4468 (1994).

[6] R. MacDonald and H. J. Eichler, Spontaneous optical pattern formation in a nematic liquid crystal with feedback mirror, Opt. Commun. **89**, 289 (1992).

[7] E. Ciaramella, M. Tamburrini, and E. Santamato, Talbot assisted hexagonal beam patterning in a thin liquid crystal film with a single feedback mirror at negative distance, Appl. Phys. Lett. **63**, 1604 (1993).

[8] T. Honda, Hexagonal pattern formation due to counterpropagation in $KNbO_3$, Opt. Lett. **18**, 598 (1993).
[9] M. Schwab, C. Denz, and M. Saffman, Multiple-pattern stability in a photorefractive feedback system, Appl. Phys. B **69**, 429 (1999).
[10] J. A. Greenberg, B. L. Schmittberger, and D. J. Gauthier, Bunching-induced optical nonlinearity and instability in cold atoms, Opt. Express **19**, 22535 (2011).
[11] G. Labeyrie, E. Tesio, P. M. Gomes, G.-L. Oppo, W. J. Firth, G. R. M. Robb, A. S. Arnold, R. Kaiser, and T. Ackemann, Optomechanical self-structuring in a cold atomic gas, Nat. Photon. **8**, 321 (2014).
[12] T. Ackemann, G. Labeyrie, G. Baio, I. Kresic, J. G. M. Walker, A. C. Boquete, P. Griffin, W. J. Firth, R. Kaiser, G.-L. Oppo, and G. R. M. Robb, Self-organization in cold atoms mediated by diffractive coupling, Atoms **9**, 35 (2021).
[13] A. Camara, R. Kaiser, G. Labeyrie, W. J. Firth, G.-L. Oppo, G. R. M. Robb, A. S. Arnold, and T. Ackemann, Optical pattern formation with a two-level nonlinearity, Phys. Rev. A **92**, 013820 (2015).
[14] G. Labeyrie, I. Kresic, G. R. M. Robb, G.-L. Oppo, R. Kaiser, and T. Ackemann, Magnetic phase diagram of light-mediated spin structuring in cold atoms, Optica **5**, 1322 (2018).
[15] I. Krešić, G. Labeyrie, G. R. M. Robb, G.-L. Oppo, P. M. Gomes, P. Griffin, R. Kaiser, and T. Ackemann, Spontaneous light-mediated magnetism in cold atoms, Commun. Phys. **1**, 33 (2018).
[16] I. Krešić, G. R. M. Robb, G. Labeyrie, R. Kaiser, and T. Ackemann, Inversion-symmetry breaking in spin patterns by a weak magnetic field, Phys. Rev. A **99**, 053851 (2019).
[17] W. J. Firth, A. Fitzgerald, and C. Paré, Transverse instabilities due to counterpropagation in Kerr media, J. Opt. Soc. Am. B **7**, 1087 (1990).
[18] O. Sandfuchs, Self-organization, amplitude equations and Fourier control in a nonlinear optical feedback system, Ph.D. thesis, University of Darmstadt, 2001.
[19] G. D'Alessandro and W. J. Firth, Spontaneous hexagon formation in a nonlinear optical medium with feedback mirror, Phys. Rev. Lett. **66**, 2597 (1991).
[20] G. D'Alessandro and W. J. Firth, Hexagonal spatial patterns for a Kerr slice with a feedback mirror, Phys. Rev. A **46**, 537 (1992).
[21] D. T. Pierce and R. L. Byer, Experiments on the interaction of light and sound for the advanced laboratory, Am. J. Phys. **41**, 314 (1973).
[22] J.-F. Schaff, T. Langen, and J. Schmiedmayer, Interferometry with atoms, Nuovo Cimento **37**, 509 (2014).
[23] D. Schneble, Y. Torii, M. Boyd, E. W. Streed, D. E. Pritchard, and W. Ketterle, The onset of matter-wave amplification in a superradiant Bose-Einstein condensate, Science **300**, 475 (2003).
[24] G. R. M. Robb and B. W. J. McNeil, Four-wave mixing with self-phase matching due to collective atomic recoil, Phys. Rev. Lett. **94**, 023901 (2005).
[25] G. Kozyreff, T. Erneux, M. Haelterman, and P. Kockaert, Fast optical self-pulsing in a temporal analog of the Kerr-slice pattern-forming system, Phys. Rev. A **73**, 063815 (2006).
[26] Y. Zhang, J. Wen, S. N. Zhu, and M. Xiao, Nonlinear Talbot effect, Phys. Rev. Lett. **104**, 183901 (2010).
[27] Y. Zhang, M. R. Belić, H. Zheng, H. Chen, C. Li, J. Song, and Y. Zhang, Nonlinear Talbot effect of rogue waves, Phys. Rev. E **89**, 032902 (2014).
[28] M. Zajnulina and M. Böhm, Temporal Talbot effect: From a quasi-linear Talbot carpet to soliton crystals and Talbot solitons, Opt. Lett. **49**, 3894 (2024).
[29] W. J. Firth, I. Kresic, G. Labeyrie, A. Camara, and T. Ackemann, Thick-medium model of transverse pattern formation in optically excited cold two-level atoms with a feedback mirror, Phys. Rev. A **96**, 053806 (2017).
[30] G. Labeyrie and U. Bortolozzo, Light self-trapping in a large cloud of cold atoms, Opt. Lett. **36**, 2158 (2011).